R. & M. No. 3278

MINISTRY OF AVIATION

AERONAUTICAL RESEARCH COUNCIL
REPORTS AND MEMORANDA

Some Applications of 'Not-So-Slender' Wing Theory to Wings with Curved Leading Edges

By L. C. Squire, Ph.D.

LONDON: HER MAJESTY'S STATIONERY OFFICE
1962
TEN SHILLINGS NET

Some Applications of 'Not-So-Slender' Wing Theory to Wings with Curved Leading Edges

By L. C. SQUIRE, Ph.D.

*Reports and Memoranda No. 3278**
July, 1960

Summary. An extension of slender-wing theory, introduced by Adams and Sears, has been applied to some problems concerned with the properties of slender, lifting, wings with curved leading edges at supersonic speeds. Two particular problems are considered. These are the calculation of the change in lift, aerodynamic centre, and load distribution on uncambered wings as the Mach number increases above $M = 1 \cdot 0$ and the calculation of the camber shape to produce a given load distribution at a given Mach number.

Where possible the results are compared with linear theory and with experimental results, and the limitations of the extension are discussed.

1. *Introduction.* Work at the Royal Aircraft Establishment on slender wings has included both experimental and theoretical work on wings with curved leading edges. Most of the theoretical work[1] has been based on slender-wing theory. Large discrepancies between this theory and experimental results[2] on some uncambered wings have been found at relatively low slenderness parameters where it had been hoped that slender-wing theory would be adequate. However, at zero slenderness parameter ($M = 1 \cdot 0$) the agreement with the measured forces is generally very good[3,4]. This lack of a reliable theory has hampered analysis of the experimental results, particularly where an accurate theoretical lift-curve slope is needed. The discrepancies between theoretical and experimental results for uncambered wings also suggest that the methods used to design cambered wings with specified properties at given supersonic Mach numbers may need to be modified if the slenderness parameter is not small.

In this Report the extension of slender-body theory due to Adams and Sears, which takes account of higher-order terms in the expansion in terms of slenderness parameter, is used to calculate the aerodynamic properties of uncambered wings at supersonic speeds and to modify the camber-design methods to include the effects of Mach number. Using existing experimental results, and some linear-theory solutions, the success of the extension for uncambered wings is considered in detail.

2. *Outline of Method.* The work in this Report is based on an integral equation derived by Adams and Sears[5] which relates the doublet strength on a lifting wing without thickness to the local wing incidence. Since, however, some of the work is directed towards extending the camber design of Weber[1] the notation used will follow Weber rather than Adams and Sears. The types of planform

* Previously issued as R.A.E. Tech. Note No. Aero. 2703—A.R.C. 22,437.

considered are shown in Fig. 1 where the co-ordinates x, y and z have been non-dimensionalised by dividing the physical dimensions by the root chord c_0. Then the equation of the leading edge is given by

$$y = s(x) = s_T g(x) \tag{1}$$

where s_T is the non-dimensional semi-span, actually the ratio of the semi-span to root chord. Also

$$g(0) = 0, \quad g(1) = 1.$$

In the notation used here the integral equation of Adams and Sears {Equation (49) of Ref. 5} becomes

$$\begin{aligned} V_0\alpha(x, y) = & -\int_{-s(x)}^{s(x)} h_{y'}(x, y')\frac{dy'}{y-y'} + \\ & + \frac{\beta^2 {s_T}^2}{2{s_T}^2}\left[(-\tfrac{1}{2}+\ln\beta s_T)\frac{d}{dx}\int_{-s(x)}^{s(x)} h_x(x, y')\,dy' + \right. \\ & + \frac{\partial}{\partial x}\int_{-s(x)}^{s(x)} h_x(x, y')\ln\left|\frac{y}{2s_T}-\frac{y'}{2s_T}\right| dy' - \\ & \left. - \frac{d^2}{dx^2}\int_0^x \ln(x-x')\,dx' \int_{-s(x')}^{s(x')} h_{x'}(x', y')\,dy'\right]. \end{aligned} \tag{2}$$

In Equation (3), $h(x, y)$ is a doublet distribution which is related to the velocity potential at the surface by

$$h(x, y) = \mp \frac{1}{\pi}\phi(x, y, \pm 0) \tag{3}$$

(Equation (46) of Ref. 5).

Within linear theory, the local load distribution on the wing $l(x, y)$ $(= -\Delta C_p)$ is related to the surface potential by

$$\begin{aligned} l(x, y) &= \frac{2}{V_0}\left\{\frac{d\phi}{dx}(x, y, +0) - \frac{d\phi}{dx}(x, y, -0)\right\} \\ &= \frac{4}{V_0}\left\{\frac{d\phi}{dx}(x, y, +0)\right\} \\ &= -\frac{4\pi}{V_0} h_x(x, y). \end{aligned} \tag{4}$$

In terms of $l(x, y)$ Equation (2) becomes:

$$\begin{aligned} \alpha(x, y) = & -\frac{1}{V_0}\int_{-s(x)}^{s(x)} h_{y'}(x, y')\frac{dy'}{y-y'} - \\ & - \frac{\beta^2 {s_T}^2}{8\pi}\left[(-\tfrac{1}{2}+\ln\beta s_T)\frac{d}{dx}\int_{-s(x)}^{s(x)} \frac{l(x, y')}{{s_T}^2}\,dy' + \right. \\ & + \frac{\partial}{\partial x}\int_{-s(x)}^{s(x)} \frac{l(x, y')}{{s_T}^2}\ln\left|\frac{y}{2s_T}-\frac{y'}{2s_T}\right| dy' - \\ & \left. - \frac{d^2}{dx^2}\int_0^x \ln(x-x')\,dx' \int_{-s(x')}^{s(x')} \frac{l(x', y')}{{s_T}^2}\,dy'\right]. \end{aligned} \tag{5}$$

This equation can be simplified by considering the three integrals in the brackets in more detail.

The first integral, $\int_{-s(x)}^{s(x)} \frac{l(x, y')}{s_T^2} dy'$, becomes

$$\frac{1}{s_T^2}\int_{-s(x)}^{s(x)} l(x, y')dy' = -\frac{1}{s_T^2}\int_{-s(x)}^{s(x)} \Delta C_p = \frac{1}{s_T^2} L(x),$$

where $L(x)$ is the cross load acting on the wing at station x.

The second integral may be written

$$\frac{1}{s_T^2}\int_{-s(x)}^{s(x)} l(x, y')\left\{\ln\left|\frac{y}{s(x)} - \frac{y'}{s(x)}\right| + \ln\frac{s(x)}{2s_T}\right\} dy' \tag{6}$$

$$= \frac{L(x)}{s_T^2}\ln\frac{g(x)}{2} + g(x)I_0(x, \eta), \tag{7}$$

where

$$I_0(x, \eta) = \int_{-1}^{1} \frac{l(x, \eta')}{s_T}\ln|\eta - \eta'|\, d\eta', \ \eta = \frac{y}{s(x)}. \tag{8}$$

The third integral becomes

$$\int_0^x \frac{L(x')}{s_T^2}\ln(x - x')\, dx'. \tag{9}$$

The derivative of this integral with respect to x is

$$\int_0^x \left\{\frac{d}{dx'}\left(\frac{L(x')}{s_T^2}\right)\right\}\ln(x - x')\, dx' \tag{10}$$

(since $L(0) = 0$)

$$= \frac{L(x)}{s_T^2}\ln x + I_1(x) \tag{11}$$

where

$$I_1(x) = \int_0^x \left\{\frac{d}{dx'}\left(\frac{L(x')}{s_T^2}\right)\right\}\ln\left(1 - \frac{x'}{x}\right) dx'. \tag{12}$$

Substitution into (5) gives:

$$\alpha(x, y) = -\frac{1}{V_0}\int_{-s(x)}^{s(x)} h_{y'}(x, y')\frac{dy'}{y - y'} -$$

$$-\frac{\beta^2 s_T^2}{8\pi}\left[\frac{d}{dx}\left\{\left(-\tfrac{1}{2} + \ln\beta s_T + \ln\frac{g(x)}{2x}\right)\frac{L(x)}{s_T^2}\right\} -\right.$$

$$\left. -\frac{d}{dx}I_1(x) + \frac{\partial}{\partial x}g(x)I_0(x, \eta)\right]. \tag{13}$$

Evaluation of the integrals I_0 and I_1 is considered in Appendix I.

Equation (13) can now be applied to the two types of problem considered in the Introduction. These are

(*a*) to find the load distribution at a given Mach number for a specified wing {$\alpha(x, y)$ given} and

(*b*) to find the shape at a given Mach number which supports a given load distribution {$h(x, y)$ or $l(x, y)$ given}.

The first of these problems involves the solution of the integral equation for $h(x, y)$. However, this is straightforward if, as suggested by Adams and Sears, $h(x, y)$ is expanded in terms of βs_T. The expansion in fact takes the form

$$h(x, y) = h^{(0)}(x, y) + \beta^2 s_T{}^2 \ln \beta s_T h^{(1)}(x, y) + \beta^2 s_T{}^2 h^{(2)}(x, y) + \\ + \text{higher-order terms.}$$

Then substitution into Equation (13) gives

$$-\frac{1}{V_0}\int_{-s(x)}^{s(x)} h_{y'}{}^{(0)}(x, y')\frac{dy'}{y-y'} = \alpha(x, y) \tag{14}$$

$$-\frac{1}{V_0}\int_{-s(x)}^{s(x)} h_{y'}{}^{(1)}(x, y')\frac{dy'}{y-y'} = \frac{1}{8\pi}\frac{d}{dx}\left(\frac{\bar{L}(x)}{s_T{}^2}\right) \tag{15}$$

$$-\frac{1}{V_0}\int_{-s(x)}^{s(x)} h_{y'}{}^{(2)}(x, y')\frac{dy'}{y-y'} = \frac{1}{8\pi}\left[\frac{d}{dx}\left\{\left(-\tfrac{1}{2} + \ln\frac{g(x)}{2x}\right)\frac{\bar{L}(x)}{s_T{}^2}\right\} - \right. \\ \left. - \frac{d}{dx}\bar{I}_1(x) + \frac{\partial}{\partial x} g(x)\bar{I}_0(x, \eta)\right] \tag{16}$$

where, in (15) and (16), $\bar{L}(x)$, $\bar{I}_1(x)$ and $\bar{I}_0(x, \eta)$ are the first terms of the expansions of $L(x)$, $I_1(x)$ and $I_0(x, \eta)$ in terms of βs_T, so that $\bar{L}(x)$, $\bar{I}_1(x)$ and $\bar{I}_0(x, \eta)$ only depend on $h'^{0)}(x, y)$. Then Equations (14), (15) and (16) can be solved successively as integral equations in which the right-hand side is known and for which the solution can be written down (*see* Appendix II). Applications of this method to various uncambered wings with different curved leading edges are considered in Section 3.

The second problem is even more straightforward since it only involves the substitution of the given load distribution into the right-hand side of Equation (13). In fact

$$\alpha(x, y) = \alpha_0(x, y) - \frac{\beta^2 s_T{}^2}{8\pi}\left[\frac{d}{dx}\left\{\left(-\tfrac{1}{2} + \ln\beta s_T + \ln\frac{g(x)}{2x}\right)\frac{L(x)}{s_T{}^2}\right\} - \right. \\ \left. - \frac{d}{dx} I_1(x) + \frac{\partial}{\partial x} g(x) I_0(x, \eta)\right] \tag{17}$$

where $\alpha_0(x, y)$ is the downwash distribution required to produce the given load at $\beta s_T = 0$, *i.e.*, the slender-wing incidence distribution. Then the change in wing shape from the shape given by slender-wing theory is

$$\Delta z(x, y) = \frac{\beta^2 s_T{}^2}{8\pi}\left[\left(-\tfrac{1}{2} + \ln\beta s_T + \ln\frac{g(x)}{2x}\right)\frac{L(x)}{s_T{}^2} + g(x) I_0(x, \eta) - \right. \\ \left. - I_1(x)\right] + f(y) \tag{18}$$

where $f(y)$ is an arbitrary function of y. Examples of this method are given in Section 5.

The accuracy of the present approach may be assessed by considering some delta wings with streamwise camber, the full linear solutions of which are known[6, 7]. In fact Adams and Sears give a graphical comparison between the results of not-so-slender and linear theory for the uncambered delta wing. This example is repeated here to show the analytical relation between the two solutions in terms of βs_T.

For this uncambered delta wing, $\alpha(x, y) = \alpha_0$, and $s(x) = s_T x$. Then the solution of Equation (14) is

$$h^{(0)}(x, \eta) = -\frac{\alpha_0 V_0}{\pi} s_T x \sqrt{(1-\eta^2)}$$

or

$$l^{(0)}(x, \eta) = \frac{4\alpha_0 s_T}{\sqrt{(1-\eta^2)}}. \tag{19}$$

Substitution into Equations (15) and (16) gives:

$$-\frac{1}{V_0}\int_{-s_T x}^{s_T x} h_{y'}^{(1)}(x, y')\frac{dy'}{y-y'} = \frac{\alpha_0}{2}$$

$$-\frac{1}{V_0}\int_{-s_T x}^{s_T x} h_{y'}^{(2)}(x, y')\frac{dy'}{y-y'} = \frac{\alpha_0}{2}\left[\tfrac{1}{2} - \ln 4\right]. \tag{20}$$

Since the right-hand sides of these equations are independent of x and y the solutions are (Appendix II):

$$h^{(1)}(x, \eta) = -\frac{\alpha_0 V_0}{2\pi} s_T x \sqrt{(1-\eta^2)}$$

$$h^{(2)}(x, \eta) = -\frac{\alpha_0 V_0}{2\pi} s_T x \sqrt{(1-\eta^2)}\left[\tfrac{1}{2} - \ln 4\right].$$

So

$$l(x, \eta) = \frac{4\alpha_0 s_T}{\sqrt{(1-\eta^2)}}\left\{1 + \tfrac{1}{2}\beta^2 s_T{}^2\left[\tfrac{1}{2} + \ln\frac{\beta s_T}{4}\right]\right\}. \tag{21}$$

But by linear theory

$$l(x, \eta) = \frac{4\alpha_0 s_T}{\sqrt{(1-\eta^2)}}\frac{1}{E}, \tag{22}$$

where E is the complete elliptic integral of the second kind of modulus $\sqrt{(1-\beta^2 s_T{}^2)}$. For small βs_T, $1/E$ may be expanded in terms of βs_T to give

$$\frac{1}{E} = 1 + \tfrac{1}{2}\beta^2 s_T{}^2\left[\tfrac{1}{2} + \ln\frac{\beta s_T}{4}\right] + \ldots . \tag{23}$$

Thus, as might be expected, linear theory and not-so-slender theory agree up to terms in $\beta^2 s_T{}^2$. Values of the lift coefficient calculated from Equations (21) and (22) are shown in Fig. 2, together with the lift coefficient given by slender-wing theory, *i.e.*, by ignoring the βs_T terms in Equation (21). Similarly it can be shown that for delta wings with local incidence distributions given by $\alpha = \alpha_i x^i$ the not-so-slender theory agrees with the full linear solution up to terms in $\beta^2 s_T{}^2$. Lift coefficients for the wings with incidence distributions $\alpha = \alpha_1 x$ and $\alpha = \alpha_2 x^2$ as given by linear, slender, and not-so-slender theory are also included in Fig. 2.

In all the comparisons of Fig. 2 it can be seen that the not-so-slender theory overestimates the effect of the parameter βs_T as compared with linear theory. Thus for these wings the terms in $\beta^4 s_T{}^4$ which are ignored in not-so-slender theory will probably be of opposite sign to the $\beta^2 s_T{}^2$ terms.

3. *Calculation of the Aerodynamic Coefficients of Flat Wings.* In this Section Equations (14), (15) and (16) are used to find the lift coefficients, aerodynamic centres and chordwise variations of cross load on some uncambered wings with curved leading edges at Mach numbers greater than 1·0.

For these wings the solution of Equation (14), that is the slender-wing lift distribution, is

$$h^{(0)}(x, \eta) = -\alpha \frac{s(x)}{\pi} V_0 \sqrt{(1-\eta^2)}, \tag{24}$$

so

$$\frac{l^{(0)}(x, \eta)}{s_T} = \frac{4\alpha g'(x)}{\sqrt{(1-\eta^2)}}, \tag{25}$$

where

$$g'(x) = \frac{d}{dx} g(x).$$

Then

$$\frac{\bar{L}(x)}{{s_T}^2} = 4\alpha\pi g(x)g'(x) \tag{26}$$

$$\bar{I}_0(x, \eta) = 4\alpha g'(x) \int_{-1}^{1} \frac{\ln|\eta - \eta'|}{\sqrt{(1-\eta'^2)}} d\eta' \tag{27}$$

$$= -4\alpha g'(x)\pi \ln 2. \quad \{See \text{ Appendix I, Equation (44)}\}$$

$$\bar{I}_1(x) = 4\pi\alpha \int_0^x \frac{d}{dx'} (g(x')g'(x')) \ln\left(1 - \frac{x'}{x}\right) dx'$$

$$= \sum i a_i b_i x^i \tag{28}$$

where the coefficients a_i are given by $\sum a_i x^i = 4\pi\alpha g(x)g'(x)$ and the coefficients $b_i = -\frac{1}{i}\sum_1^i \frac{1}{r}$ (*see* Appendix I).

Substitution of (26), (27) and (28) into Equations (15) and (16) then gives

$$-\frac{1}{V_0} \int_{-s(x)}^{s(x)} h_{y'}{}^{(1)}(x, y') \frac{dy'}{y - y'} = \frac{\alpha}{2} \{g'(x)g'(x) + g(x)g''(x)\}$$

$$= \alpha G(x), \text{ (say)} \tag{29}$$

and

$$-\frac{1}{V_0} \int_{-s(x)}^{s(x)} h_{y'}{}^{(2)}(x, y') \frac{dy'}{y - y'}$$

$$= \frac{\alpha}{2} \left[\left(-\frac{1}{2} + \ln \frac{g(x)}{4x} \right) (g'(x)g'(x) + g(x)g''(x)) + g'(x)g'(x) - \right.$$

$$\left. - \frac{g(x)g'(x)}{x} - \frac{1}{4\pi\alpha} \sum i^2 a_i b_i x^{i-1} \right]$$

$$= \alpha F(x), \text{ (say)}. \tag{30}$$

Thus

$$h^{(1)}(x,\eta) = -\alpha G(x)\frac{s(x)}{\pi}V_0\sqrt{(1-\eta^2)} \tag{31}$$

$$h^{(2)}(x,\eta) = -\alpha F(x)\frac{s(x)}{\pi}V_0\sqrt{(1-\eta^2)} \tag{32}$$

so

$$h(x,\eta) = -\alpha\{1+\beta^2 s_T{}^2F(x)+\beta^2 s_T{}^2G(x)\ln\beta s_T\}\frac{s(x)}{\pi}V_0\sqrt{(1-\eta^2)} \tag{33}$$

and

$$\begin{aligned}\frac{l(x,\eta)}{s_T} &= 4\alpha\{1+\beta^2 s_T{}^2F(x)+\beta^2 s_T{}^2G(x)\ln\beta s_T\}\frac{g'(x)}{\sqrt{(1-\eta^2)}}+\\ &\quad+4\alpha\{\beta^2 s_T{}^2F'(x)+\beta^2 s_T{}^2G'(x)\ln\beta s_T\}g(x)\sqrt{(1-\eta^2)}.\end{aligned} \tag{34}$$

Then the cross load $L(x)$ is

$$\begin{aligned}\frac{L(x)}{s_T{}^2} &= 4\alpha\pi g(x)g'(x)\{1+\beta^2 s_T{}^2F(x)+\beta^2 s_T{}^2G(x)\ln\beta s_T\}+\\ &\quad+2\alpha\pi g^2(x)\{\beta^2 s_T{}^2F'(x)+\beta^2 s_T{}^2G'(x)\ln\beta s_T\}\\ &= 2\alpha\pi\frac{d}{dx}\{g^2(x)(1+\beta^2 s_T{}^2F(x)+\beta^2 s_T{}^2G(x)\ln\beta s_T)\}.\end{aligned} \tag{35}$$

By integration of (35) the lift coefficient, C_L, is

$$C_L = \frac{\pi}{2}A\alpha[1+\beta^2 s_T{}^2F(1)+\beta^2 s_T{}^2G(1)\ln\beta s_T] \tag{36}$$

where A = aspect ratio = $4s_T{}^2/\text{area}$.
The centre of pressure position, $\bar{x}$, is given by

$$\begin{aligned}\bar{x} &= \int_0^1 xL(x)dx\Big/\int_0^1 L(x)dx\\ &= 1-\frac{\int_0^1 g^2(x)(1+\beta^2 s_T{}^2F(x)+\beta^2 s_T{}^2G(x)\ln\beta s_T)dx}{1+\beta^2 s_T{}^2F(1)+\beta^2 s_T{}^2G(1)\ln\beta s_T}.\end{aligned} \tag{37}$$

Using results (35), (36) and (37), $(2/\pi A)(\partial C_L/\partial\alpha)$, $\bar{x}$ and $L(x)/2\pi\alpha s_T{}^2$ are plotted against βs_T in Figs. 3 to 11 for the three planforms shown in Fig. 1 and defined by:

$$g(x) = x(2-x) \qquad \text{'gothic',}$$

$$g(x) = \frac{5}{4}x\left(1-\frac{x^4}{5}\right) \qquad \text{'modified gothic',}$$

$$g(x) = x\left(1-\frac{3}{2}x+4x^2-\frac{5}{2}x^3\right) \qquad \text{'ogee'.}$$

In the next section the results for the gothic and ogee wing are compared with some experimental results. Before this comparison is made the probable accuracy of the present theory as applied to these planforms will be considered. With increase in βs_T, the load at the front of the wings decreases (Figs. 5, 8 and 11) and, in view of the comparisons of Fig. 2, it seems probable that this decrease is overestimated by not-so-slender theory. As pointed out in Section 2 this implies that the terms of order $\beta^4 s_T{}^4$ which are ignored in not-so-slender theory are of opposite sign to the terms of order $\beta^2 s_T{}^2$ which are included. If, as seems likely, the ignored terms remain of opposite sign to the terms

of order $\beta^2 s_T^2$ over the whole wing, then the increase in load at the rear of these planforms with βs_T will be overestimated. Without a full linear-theory solution for one of these planforms, which is not available at the moment, this error cannot be accurately assessed. However, it appears reasonable to assume that if the differences between the results given by slender-wing theory and those given by not-so-slender theory are small, then the errors in these differences will be negligibly small. Thus the load distributions for the gothic wing, Fig. 5, suggest that up to about $\beta s_T = 0{\cdot}4$ not-so-slender theory will give fairly accurate results whereas on the ogee wing, Fig. 11, the large changes in load distribution at the trailing edge, even at $\beta s_T = 0{\cdot}2$, suggest that large errors due to neglecting higher-order terms are present. It should be noted, however, that even if the neglected terms are large the trends shown by not-so-slender theory are probably still valid.

It appears, from the results plotted in Figs. 5, 8 and 11, that the changes due to not-so-slender theory increase as the higher streamwise derivatives of $L(x)$ increase in magnitude {as can also be shown from the general solution for $L(x)$, Equation (35)}. Thus the range of applicability of not-so-slender theory will probably decrease with increase in magnitude of these derivatives.

4. *Comparison of the Flat-Wing Calculations with Experimental Results.* In comparing the calculations of Section 3 with experiment a difficulty arises in that, to achieve low values of βs_T, the wings must be geometrically slender and so leading-edge separations, which modify the load distributions and introduce non-linearities in the lift and moment curves, occur in practice at low incidence. In the experimental results[2, 3, 4] these non-linearities make the evaluation of lift-curve slope and aerodynamic centre at zero incidence rather inaccurate. Hence, instead of the experimental lift-curve slope and aerodynamic centre being compared with theory, the experimental results have been plotted and the linear results as given by slender, and not-so-slender, theory have been superimposed on these plots. The comparisons are made in Figs. 12 and 13 for a gothic wing[2, 3] of aspect ratio $0{\cdot}75$ at Mach numbers between $1{\cdot}02$ and $2{\cdot}0$ and in Figs. 14 and 15 for an ogee wing[4] of aspect ratio $1{\cdot}2$ at Mach numbers from $1{\cdot}02$ to $1{\cdot}6$.

4.1. *Gothic Wing.* In Fig. 12 it can be seen that the linear lift as given by not-so-slender theory is in good agreement with the experimental lift at low incidence for values of βs_T up to about $0{\cdot}3$ but above this value the experimental lift lies between the lifts as given by slender and not-so-slender theory, confirming that at these values of βs_T the effects of Mach number are overestimated by not-so-slender theory.

Before comparing aerodynamic centres for the gothic planform it should be noted that the experiments were made on a thick wing ($8{\cdot}4$ per cent at the root chord) and that the effect of this thickness is to move the aerodynamic centre aft of the thin-wing position. Also the results at $M = 1{\cdot}02$ may be subject to wind-tunnel interference[3]. Taken together these facts reduce the value of any detailed discussion of Fig. 13. The most that can be said is that between $\beta s_T = 0{\cdot}25$ and $\beta s_T = 0{\cdot}433$ the experimental aerodynamic centre moves back by about 4 per cent of the root chord as compared with the theoretical shift of $5{\cdot}7$ per cent. It should be noted that the discussion in Section 3 suggests that the linear-theory movement in aerodynamic centre will be less than that given by not-so-slender theory.

4.2. *Ogee Wing.* The experimental results for the ogee wing of aspect ratio $1{\cdot}2$ (Figs. 14 and 15) are not in good agreement with the not-so-slender-theory values, although the results at $M = 1{\cdot}02$ are in close agreement with the slender-theory values. However, the lowest experimental value of

βs_T (other than 0·06) is 0·225, since at Mach numbers between 1·02 and 1·25 the model may be subject to large and mainly unknown interference effects. Thus the range of slenderness parameter for which Fig. 11 suggests that not-so-slender theory will give good results is excluded from the comparison with experimental results.

For this planform the changes in $L(x)$ predicted by not-so-slender theory (Fig. 11) are extremely large towards the trailing edge and so it is not surprising that the neglect of the higher-order terms leads to large errors. The errors in slender-wing theory will be even greater and so the agreement with this theory at the higher values of βs_T is clearly fortuitous.

It should be noted that if this planform were cambered so that $L(x)$ became a smoother function of x (*i.e.*, $\{L(x)\}_{\max}$ moved forward) then the range of applicability of not-so-slender theory would probably be increased (*see* Section 5.2).

5. *Calculation of the Shape of a Cambered Wing for a Given Load Distribution.* 5.1. *Details of Calculation.* As stated in the Introduction the object of this Section is to modify the camber-design method of Weber[1] to include the effects of Mach number. Weber's method aims to produce a cambered wing such that at the design lift and design Mach number the following conditions are satisfied:

(*a*) There is zero load at the leading edge; this is in order to obtain attached flow.

(*b*) The drag due to lift is low; this puts conditions on the spanwise and chordwise loadings.

(*c*) The centre of pressure is at a fixed position.

(*d*) The pressure gradients caused by camber must not be sufficiently adverse to produce boundary-layer separations on the wing.

Weber has given a set of load distributions, designed to satisfy these conditions, in terms of three parameters: ν (which varies from 1 to 3), $\eta_0(x)$ and $C(x)$. The wing shapes which produce these load distributions were calculated by slender-wing theory. In fact the incidence distribution as given by slender-wing theory is

$$\alpha(x, \eta) = C(x) \text{ for } 0 \leqslant |\eta| \leqslant \eta_0(x) \tag{38}$$

$$\alpha(x, \eta) = C(x) + D_\nu(x)\left[\frac{|\eta| - \eta_0(x)}{1 - \eta_0(x)}\right]^{\nu-1} \text{ for } \eta_0(x) \leqslant |\eta| \leqslant 1 \tag{39}$$

where $\eta = y/s(x)$ and $D_\nu(x)$ is a given function of ν, $\eta_0(x)$ and $C(x)$.

We wish to modify this slender-wing shape by including the not-so-slender terms. Formally this modification is found simply by substituting the given load distribution into Equation (18) and carrying out the integrations. In practice, however, these integrations, particularly for $I_0(x, \eta)$ and $I_1(x)$, are extremely difficult, owing to the complex nature of the load distributions {*see* Ref. 1, Equations (32), (33) and (34)}. Thus it is necessary to find suitable approximations for $l(x, \eta)$ and $L(x)$ which reduce $I_0(x, \eta)$ and $I_1(x)$ to manageable forms. A study of Weber's solutions suggests that $l(x, \eta)$ and $L(x)$ can be reduced to the approximate forms:

$$\frac{l(x, \eta)}{s_T} = \sum_i n_i(x)\eta^{2i}\sqrt{(1-\eta^2)}, \tag{40}$$

$$\frac{L(x)}{s_T{}^2} = \sum_i a_i x^i. \tag{41}$$

The evaluation of $I_0(x, \eta)$ and $I_1(x)$ with these approximate forms is given in Appendix I.

5.2. *Discussion of Example.* As an example the method has been applied to a cambered wing of modified gothic planform (Fig. 1). Tests were made on two models with the same design load distribution, one wing being designed by slender-wing theory and the other by not-so-slender theory for a slenderness parameter of 0·4. The wing shape, as given by slender-wing theory (which ignores the βs_T terms), is given in Fig. 16, while the design load distributions and the approximations used in Equation (18) are illustrated in Fig. 17. The new wing shape obtained by including the not-so-slender terms at $\beta s_T = 0{\cdot}4$ ($M = 1{\cdot}89$ for this wing) is compared with the original slender-wing-theory shape in Fig. 18. The main part of this figure illustrates the shapes of the centre-lines and leading edges of the two wings (note the exaggerated vertical scale) while the insert shows the effects of the not-so-slender terms on two typical cross-sections. It should be noted that although the change in shape due to including the not-so-slender terms appears small the changes in local incidence are more significant.

In Fig. 19 the chordwise variation of spanwise load, as calculated by not-so-slender theory, is shown for the two wings at $\beta s_T = 0$ and $\beta s_T = 0{\cdot}4$. It should be remembered that the load at $\beta s_T = 0$ on the wing designed by slender-wing theory is the design load and so is equal to that at $\beta s_T = 0{\cdot}4$ on the modified wing. The main point of interest in these loads is that the changes with slenderness parameter are smaller for these cambered wings than for the uncambered wing of the same planform (*see* Fig. 8). These smaller changes are due to the smoother variation of $L(x)$ for the cambered wing, particularly over the rear region of the wing.

The main experimental results of interest in the present work are presented on Fig. 20. Here the centre-of-pressure positions of the two wings at $C_L = 0{\cdot}05$ (the design lift coefficient) are plotted against βs_T; the figure also includes the design positions and the variation of the position as calculated by not-so-slender theory. It will be seen that at the higher values of βs_T the experimental and theoretical positions are in excellent agreement whereas near $\beta s_T = 0$ the measured positions are ahead of the calculated positions. This lack of agreement near $\beta s_T = 0$ could be to a thickness effect in which case the good agreement at higher values of βs_T might be fortuitous. In spite of this the results do suggest that for this planform not-so-slender theory provides a reasonable method of designing wings with a given centre-of-pressure position at supersonic speeds.

Near the design Mach numbers of the two wings the design C_L (0·05) was achieved close to the design incidence, but there is some evidence that on the not-so-slender wing the condition of zero leading-edge load was not reached until $C_L = 0{\cdot}070$.

6. *Conclusions.* The extension to slender-wing theory, known as 'not-so-slender' theory, proposed by Adams and Sears[5] has been used to derive formulae for the calculation of the properties of slender wings with curved leading edges at supersonic speeds and to modify the camber design methods of Weber[1] to include Mach number effects.

The extension gives the load distributions, or the shape for a given load, correct to order $\beta^2 s_T^2$. A comparison of the extension with full linear theory for some cambered delta wings shows that not-so-slender theory tends to overestimate the effects of Mach number. Experimental results for some wings with curved leading edges, for which no linear solution is available, also suggest that the effects of Mach number are overestimated by the theory. In general the range of applicability of not-so-slender theory appears to depend on the magnitude of the higher streamwise derivatives of the spanwise load, the range decreasing with increase in the magnitude of these derivatives.

LIST OF SYMBOLS

a_i		Coefficients of power series {Equations (28), (41)}
b_i		Appendix I
c_0		Root chord
$f(y)$		Arbitrary function of integration {Equation (18)}
$g(x)$	$=$	$s(x)/s_T$
$h(x, y)$		Doublet distribution {Equation (3)}
k	$=$	$\sqrt{(1-\beta^2 s_T{}^2)}$
$l(x, y)$		Local load distribution
$n_i(x)$		Functions of x {Equation (40) and Appendix I}
$s(x)$		Local semi-span
s_T		Semi-span at trailing edge; ratio of semi-span to root chord
x, y, z		Cartesian co-ordinates; origin at wing apex; x along the free-stream direction, y spanwise, z positive upwards; all are made dimensionless with the root chord
$z(x, y)$		Ordinate of wing surface
A		Aspect ratio
C_p		Pressure coefficient
$C(x)$	$=$	$-\partial z(x, 0)/dx$, downwash at centre section
$D_\nu(x)$		Parameter in downwash {Equation (39)}
$E(k)$		Complete elliptic integral of second kind
$F(x)$, $G(x)$		Functions defined in Equations (29) and (30)
$I_0(x, \eta)$		*See* Equation (8)
$I_1(x)$		*See* Equation (12)
$L(x)$		Spanwise (or cross) load
M_0		Mach number (free stream)
V_0		Free-stream velocity
$\alpha(x, y)$		Incidence
$\Delta\alpha(x, y)$		Change in incidence due to change in design βs_T
β	$=$	$\sqrt{(1-M_0{}^2)}$
η	$=$	$y/s(x)$
$\eta_0(x)$		Parameter in downwash {Equation (39)}

REFERENCES

No.	*Author*	*Title, etc.*
1	J. Weber	Design of warped slender wings with the attachment line along the leading edge. A.R.C. 20,051. September, 1957.
2	L. C. Squire	An experimental investigation at supersonic speeds of the characteristics of two gothic wings, one plane and one cambered. A.R.C. R. & M. 3211. May, 1959.
3	L. C. Squire	Further experimental investigations of the characteristics of cambered gothic wings at Mach numbers from 0·4 to 2·0. A.R.C. 23,724. December, 1961.
4	L. C. Squire and D. S. Capps ..	An experimental investigation of the characteristics of an ogee wing from $M = 0{\cdot}4$ to $M = 1{\cdot}8$. A.R.C. C.P. 585. August, 1959.
5	Mac.C. Adams and W. R. Sears ..	Slender-body theory—review and extension. *J. Ae. Sci.* Vol. 20. No. 2. February, 1953.
6	G. M. Roper	Drag reduction of thin wings at supersonic speeds, by the use of camber and twist. A.R.C. R. & M. 3132. July, 1957.
7	G. N. Lance	The delta wing in a non-uniform supersonic stream. *Aero. Quart.* Vol. V. pp. 55 to 72. May, 1954.

APPENDIX I

Evaluation of the Integrals $I_0(x, \eta)$ and $I_1(x)$

(i) $$I_0(x, \eta) = \int_{-1}^{1} \frac{l(x, \eta')}{s_T} \ln|\eta - \eta'| \, d\eta' .$$

All the local load distributions considered in this Report may be written as, or approximated by,

$$\frac{l(x, \eta)}{s_T} = \frac{m(x)}{\sqrt{(1-\eta^2)}} + \sum_0 n_i(x)\eta^{2i} \sqrt{(1-\eta^2)} . \tag{42}$$

Thus

$$I_0(x, \eta) = m(x) \int_{-1}^{1} \frac{\ln|\eta - \eta'|}{\sqrt{\{1-(\eta')^2\}}} d\eta' + \sum_0 n_i(x) \int_{-1}^{1} (\eta')^{2i} \sqrt{\{1-(\eta')^2\}} \ln|\eta - \eta'| \, d\eta' . \tag{43}$$

The integrals in (43) corresponding to $m(x)$ and $n_0(x)$ have been evaluated by Weber to give

$$\int_{-1}^{1} \frac{\ln|\eta - \eta'|}{\sqrt{\{1-(\eta')^2\}}} d\eta' = -\pi \ln 2 \tag{44}$$

and

$$\int_{-1}^{1} \sqrt{\{1-(\eta')^2\}} \ln|\eta - \eta'| \, d\eta' = \pi \left\{ \frac{\eta^2}{2} - \frac{1}{4} - \frac{1}{2} \ln 2 \right\} . \tag{45}$$

For $i > 0$ the integral $\int_{-1}^{1} (\eta')^{2i} \sqrt{\{1-(\eta')^2\}} \ln|\eta - \eta'| \, d\eta' = I_{0,i}(\eta)$, (say)

may be determined by first considering its derivative with respect to η:

$$\frac{dI_{0,i}(\eta)}{d\eta} = \int_{-1}^{1} \frac{(\eta')^{2i} \sqrt{\{1-(\eta')^2\}}}{\eta - \eta'} d\eta' \tag{46}$$

$$= \int_0^{\pi} \frac{\cos^{2i}\theta \sin^2\theta}{\cos\phi - \cos\theta} d\theta \tag{47}$$

if $\eta = \cos\phi$, $\eta' = \cos\theta$.

Expanding $\cos^{2i}\theta \sin^2\theta$ in terms of cosines of multiple angles and using the integration formula

$$\int_0^{\pi} \frac{\cos n\theta d\theta}{\cos\theta - \cos\phi} = \pi \frac{\sin n\phi}{\sin\phi}$$

$$\frac{dI_{0,i}(\eta)}{d\eta} = \pi \left(\eta^3 - \frac{1}{2}\eta \right) \qquad \text{for } i = 1, \tag{48}$$

$$= \pi \left(\eta^5 - \frac{1}{2}\eta^3 - \frac{1}{8}\eta \right) \qquad \text{for } i = 2, \tag{49}$$

$$= \pi \left(\eta^7 - \frac{1}{2}\eta^5 - \frac{1}{8}\eta^3 - \frac{1}{16}\eta \right) \qquad \text{for } i = 3 . \tag{50}$$

Then

$$I_{0,i}(\eta) = \int_0^{\eta} \frac{dI_{0i}(\eta)}{d\eta} d\eta + I_{0i}(\eta = 0), \tag{51}$$

where

$$I_{0,i}(\eta = 0) = \int_{-1}^{1} (\eta')^{2i} \sqrt{\{1 - (\eta')^2\}} \ln|\eta'| \, d\eta' \tag{52}$$

$$= \pi \left(\frac{1}{32} - \frac{1}{8}\ln 2\right) \qquad \text{for } i = 1 \tag{53}$$

$$= \pi \left(\frac{5}{192} - \frac{1}{16}\ln 2\right) \qquad \text{for } i = 2 \tag{54}$$

$$= \pi \left(\frac{59}{3072} - \frac{5}{128}\ln 2\right) \qquad \text{for } i = 3. \tag{55}$$

Thus using Equation (51)

$$I_0(x, \eta) = n_1(x) \frac{\pi}{32} \{8\eta^4 - 8\eta^2 + 1 - 4\ln 2\} \tag{56}$$

$$= n_2(x) \frac{\pi}{192} \{32\eta^6 - 24\eta^4 - 12\eta^2 + 5 - 12\ln 2\} \tag{57}$$

$$= n_3(x) \frac{\pi}{3072} \{384\eta^8 - 256\eta^6 - 96\eta^4 - 96\eta^2 + 59 - 120\ln 2\} \tag{58}$$

for

$$\frac{l(x, \eta)}{s_T} = \sum_1 n_i(x) \eta^{2i} \sqrt{\{1 - \eta^2\}}.$$

(ii) $$I_1(x) = \int_0^x \frac{d}{dx'} \left\{\frac{L(x')}{{s_T}^2}\right\} \ln\left(1 - \frac{x'}{x}\right) dx'.$$

For the uncambered wings considered in Section 3, $L(x)/{s_T}^2$ is a polynomial in x, while the cross loads considered in Section 5 may be approximated to this form.
Thus

$$\frac{L(x)}{{s_T}^2} = \sum_1^n a_i x^i. \tag{59}$$

Then

$$I_1(x) = \sum_1^n i a_i \int_0^x (x')^{i-1} \ln\left(1 - \frac{x'}{x}\right) dx' \tag{60}$$

$$= \sum_1^n i a_i x^i \int_0^1 t^{i-1} \ln(1 - t) \, dt \tag{61}$$

$$= \sum_1^n i a_i b_i x^i, \tag{62}$$

where

$$b_i = -\frac{1}{i} \sum_{r=1}^{i} \frac{1}{r}. \tag{63}$$

APPENDIX II

Solutions of the Integral Equation $-\frac{1}{V_0}\int_{-s(x)}^{s(x)} h_{y'}(x, y')\frac{dy'}{y-y'} = f(x, y)$

The solution of this equation may be written (*see*, for example, Ref. 1)

$$h(x, y) = -\frac{s(x)V_0}{\pi^2}\int_0^{\pi} f(\theta', x)\sin\theta' \ln\frac{\sin\left|\frac{\theta-\theta'}{2}\right|}{\sin\frac{\theta+\theta'}{2}}\,d\theta', \tag{64}$$

where $\cos\theta = y/s(x) = \eta$.

The forms of $f(x, y)$ considered in this Report are:

$$f(x, y) = \sum_0^n a_i(x)\left(\frac{y}{s(x)}\right)^{2i}$$

$$= \sum_0^n a_i(x)\eta^{2i}. \tag{65}$$

Thus

$$h(x, y) = -\frac{s(x)}{\pi^2}V_0\sum_0^n a_i(x)P_i, \tag{66}$$

where

$$P_i = \int_0^{\pi}\cos^{2i}\theta'\sin\theta'\ln\frac{\sin\left|\frac{\theta-\theta'}{2}\right|}{\sin\frac{(\theta+\theta')}{2}}\,d\theta'. \tag{67}$$

Values of P_i for $i = 0, 1, 2, 3$ are

$$P_0 = \pi\sqrt{(1-\eta^2)}, \tag{68}$$

$$P_1 = \frac{\pi}{6}(1+2\eta^2)\sqrt{(1-\eta^2)}, \tag{69}$$

$$P_2 = \frac{\pi}{40}(3+4\eta^2+8\eta^4)\sqrt{(1-\eta^2)}, \tag{70}$$

$$P_3 = \frac{\pi}{112}(5+6\eta^2+8\eta^4+16\eta^6)\sqrt{(1-\eta^2)}. \tag{71}$$

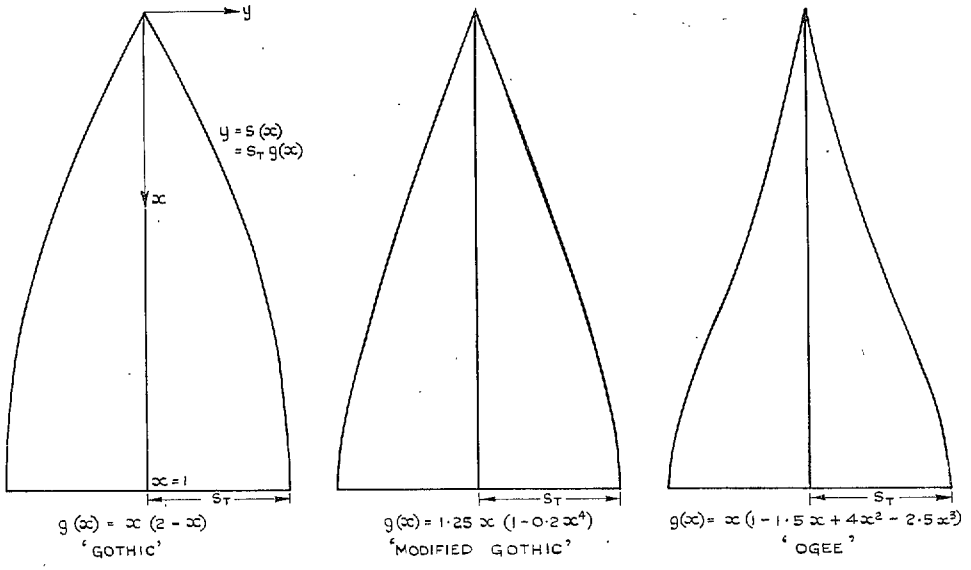

FIG. 1. Details of planforms.

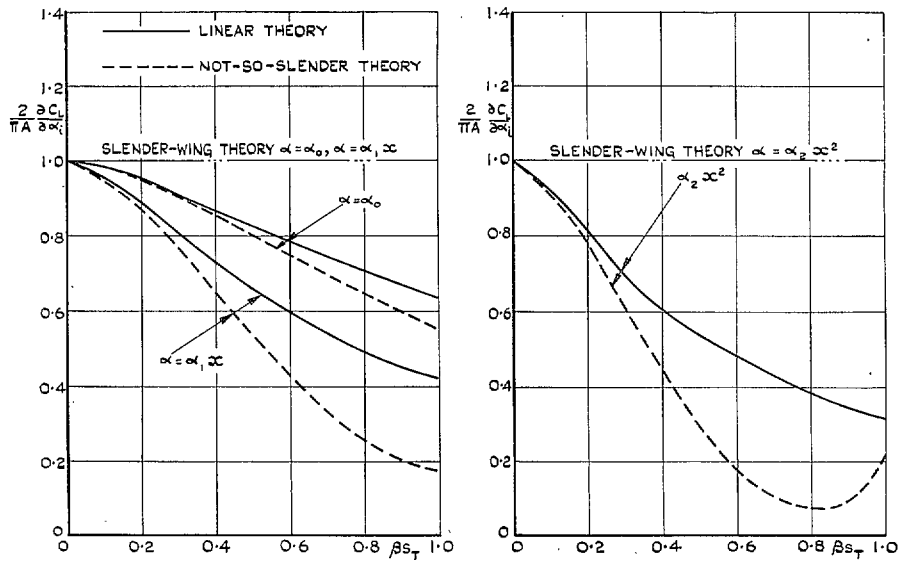

FIG. 2. Comparison of the lift-curve slopes of some delta wings as given by slender, 'not-so-slender' and linear theory.

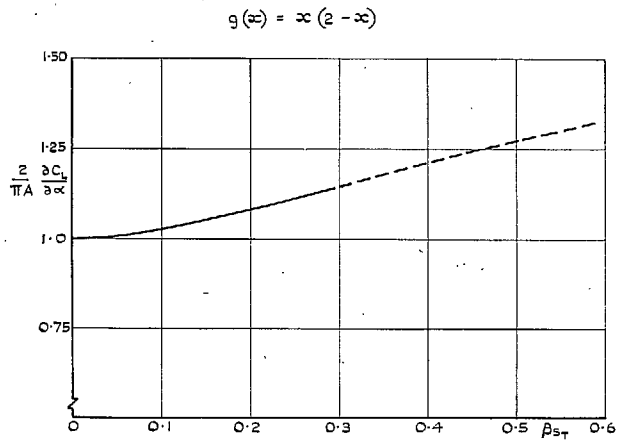

FIG. 3. Variation of gothic-wing lift-curve slope with slenderness parameter.

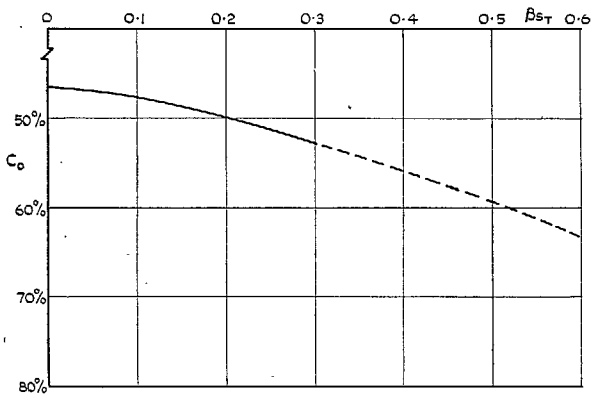

FIG. 4. Variation of gothic-wing aerodynamic centre with slenderness parameter.

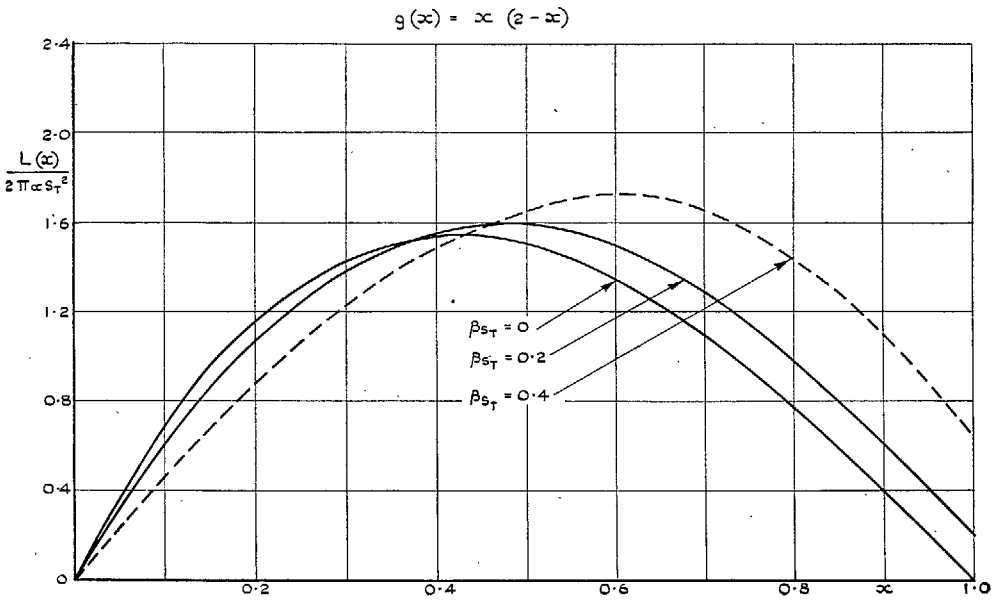

FIG. 5. Chordwise variation of spanwise load on gothic wings.

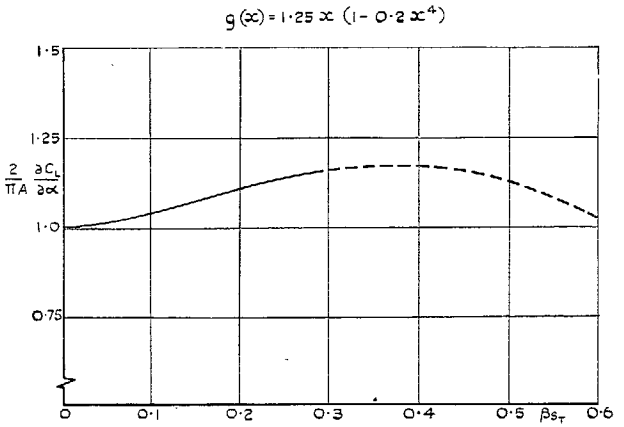

FIG. 6. Variation of modified gothic-wing lift-curve slope with slenderness parameter.

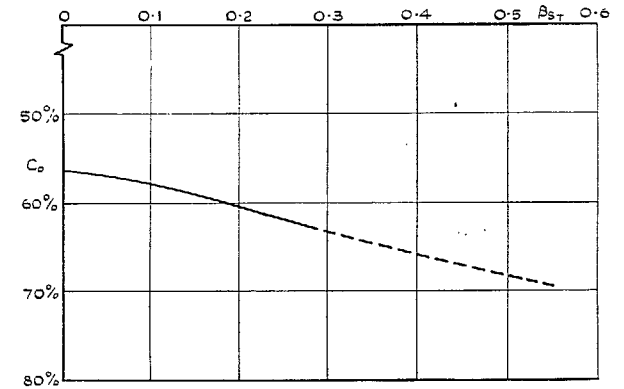

FIG. 7. Variation of modified gothic-wing aerodynamic centre with slenderness parameter.

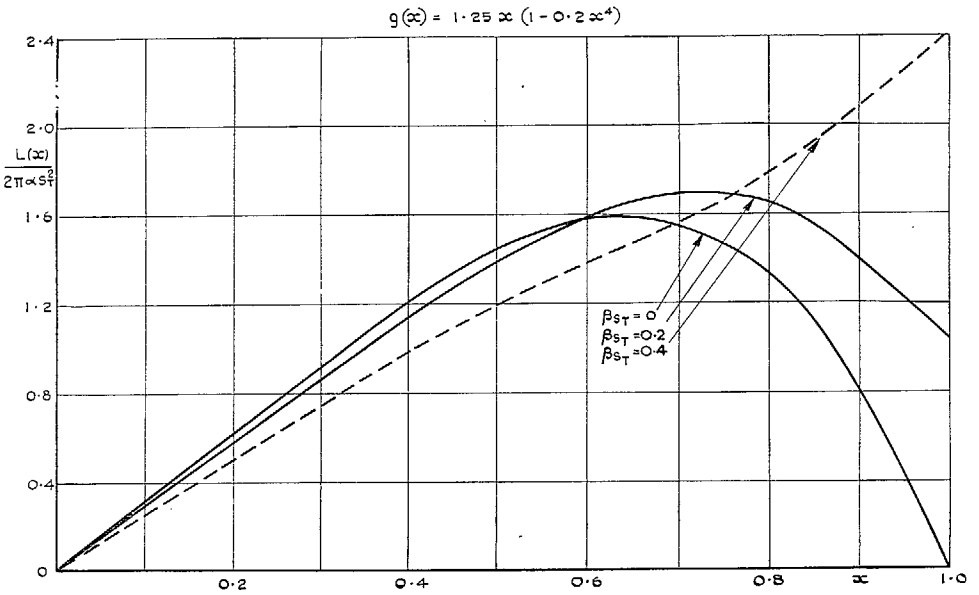

FIG. 8. Chordwise variation of spanwise load on modified gothic wings.

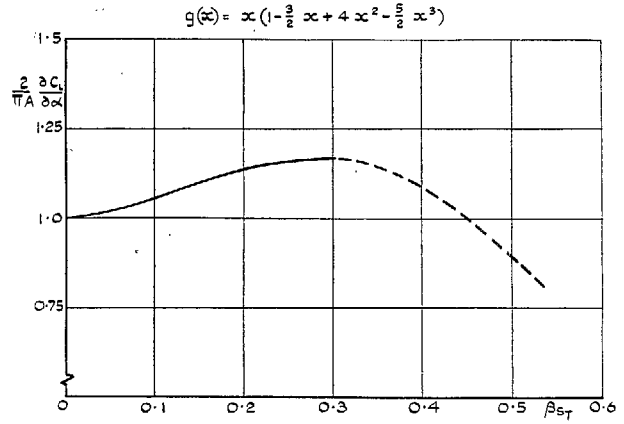

FIG. 9. Variation of ogee-wing lift-curve slope with slenderness parameter.

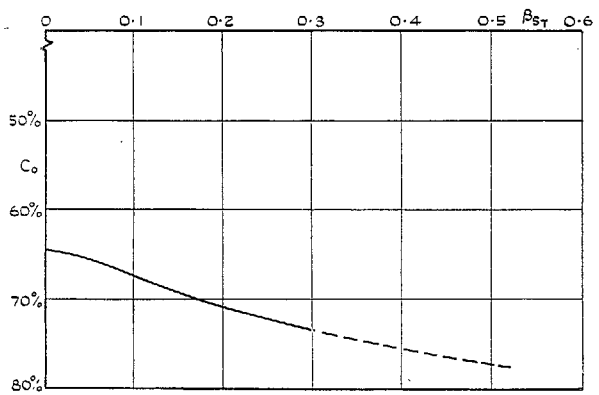

FIG. 10. Variation of ogee-wing aerodynamic centre with slenderness parameter.

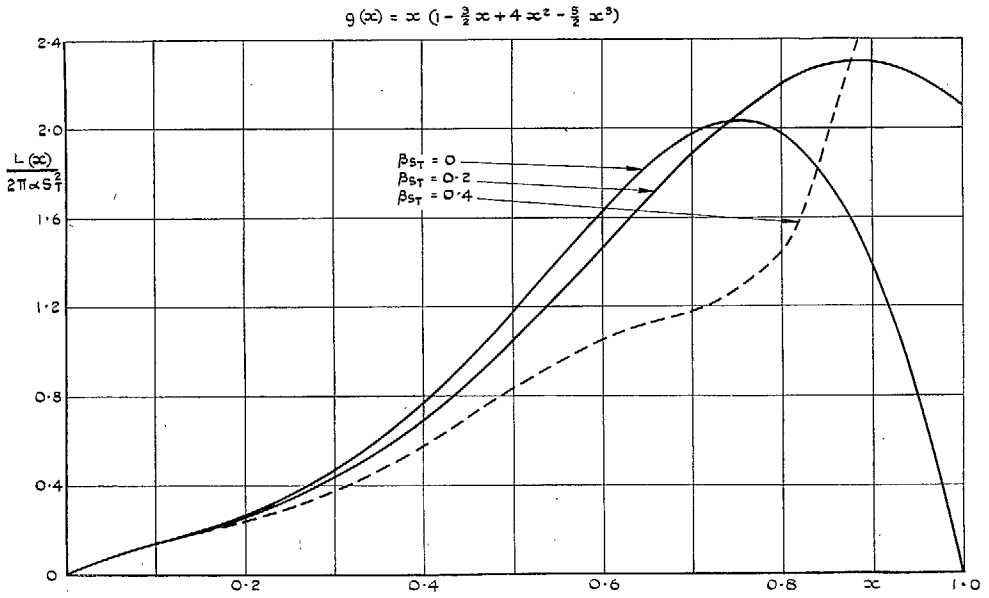

FIG. 11. Chordwise variation of spanwise load on ogee wings.

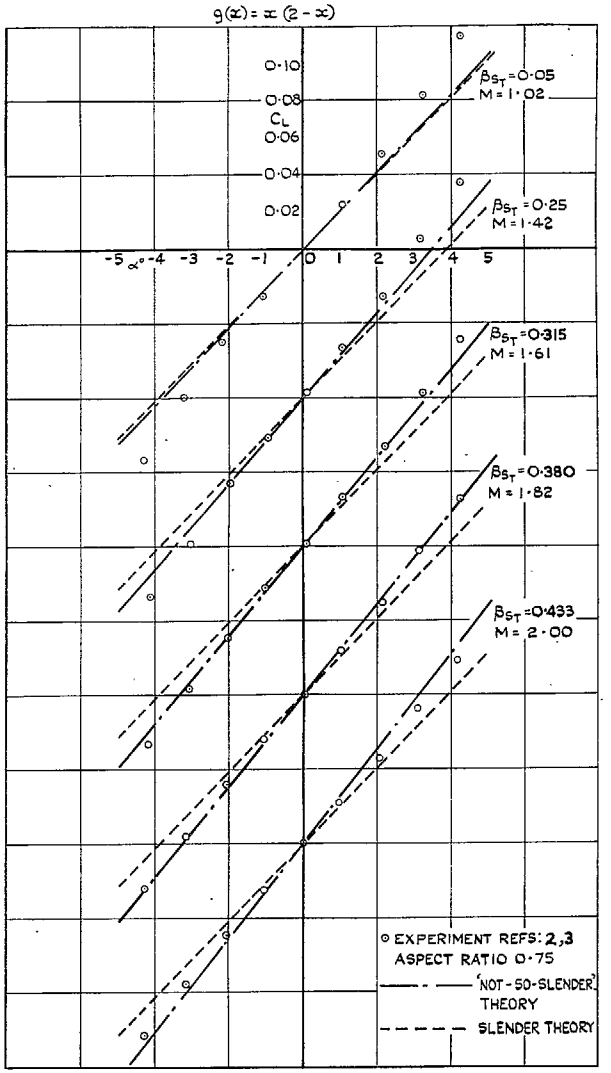

FIG. 12. Comparison of experimental and theoretical lift of an uncambered gothic wing.

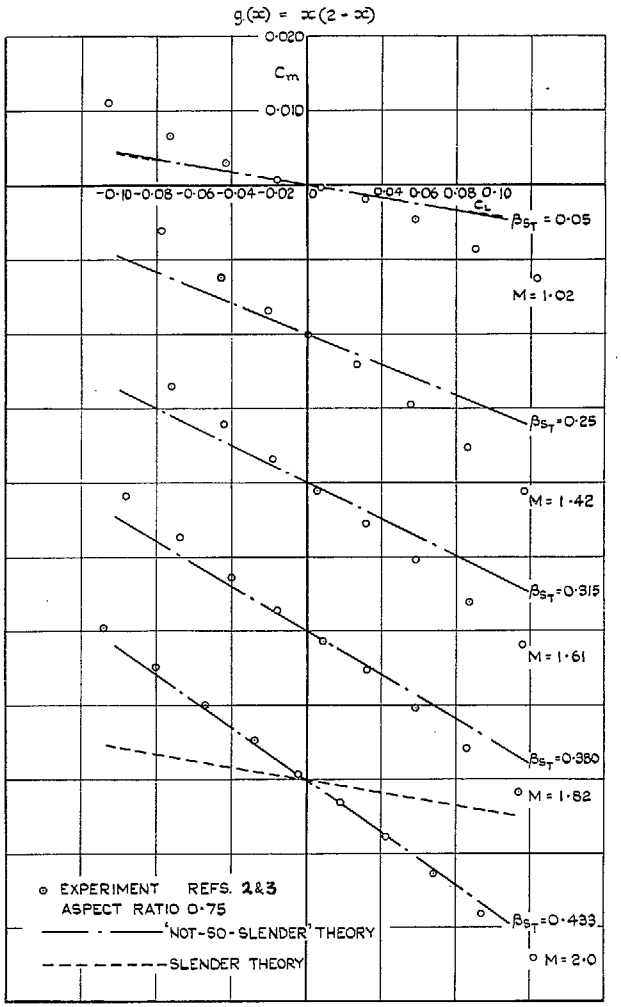

FIG. 13. Comparison of experimental and theoretical pitching moment of an uncambered gothic wing.

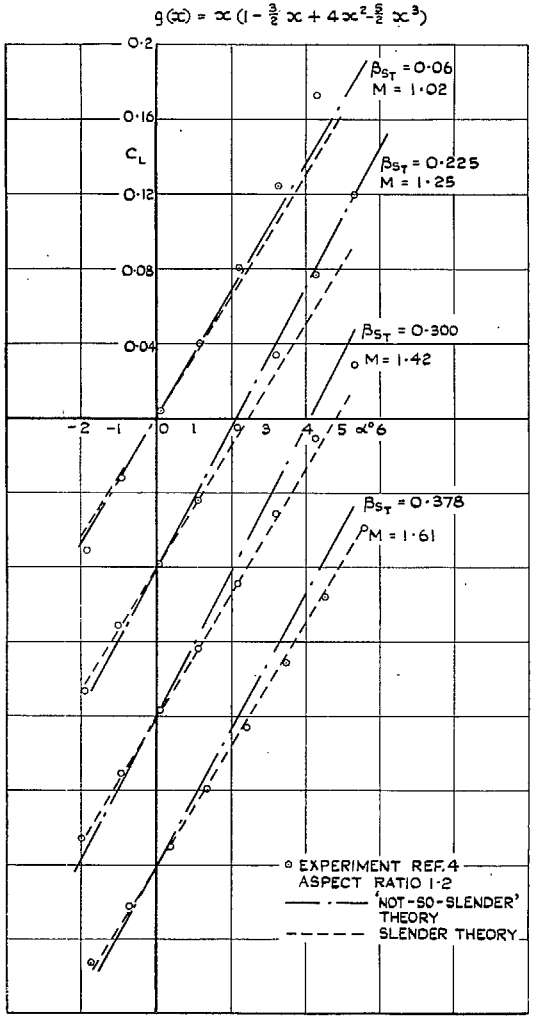

FIG. 14. Comparison of experimental and theoretical lift of an uncambered ogee wing.

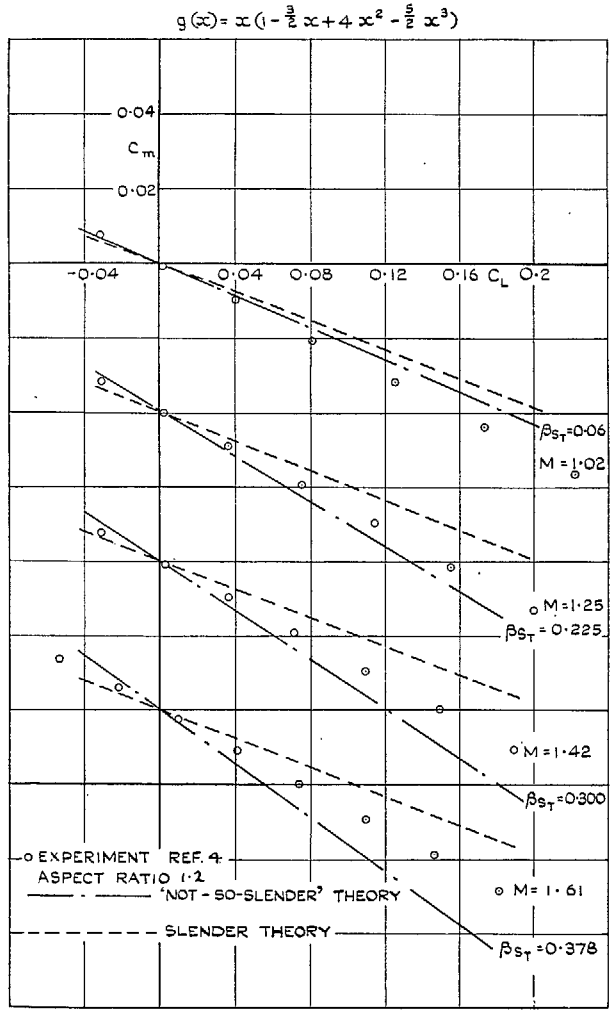

FIG. 15. Comparison of experimental and theoretical pitching moment of an uncambered ogee wing.

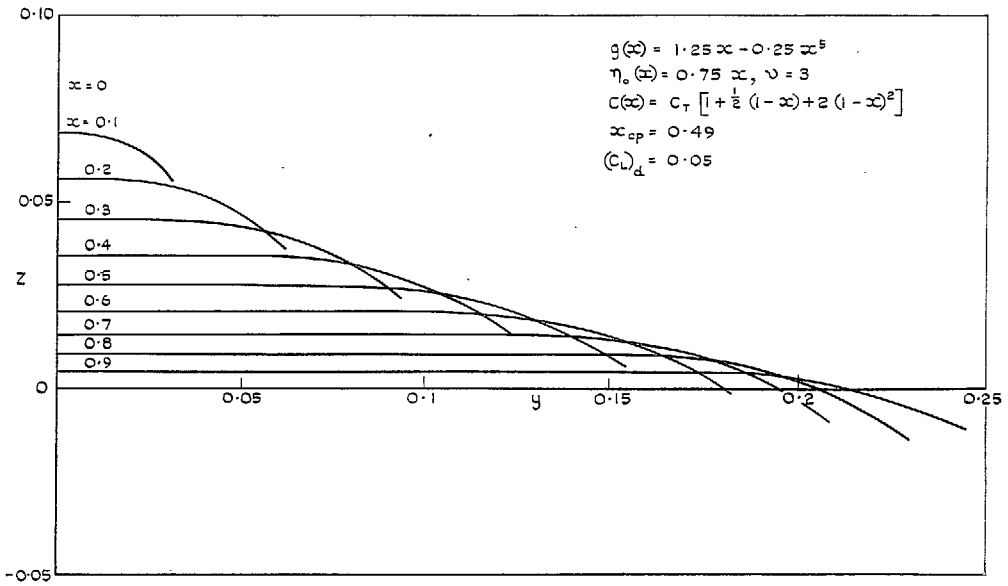

FIG. 16. Camber lines (spanwise) for example of section 5.2 ($\beta s_T = 0$).

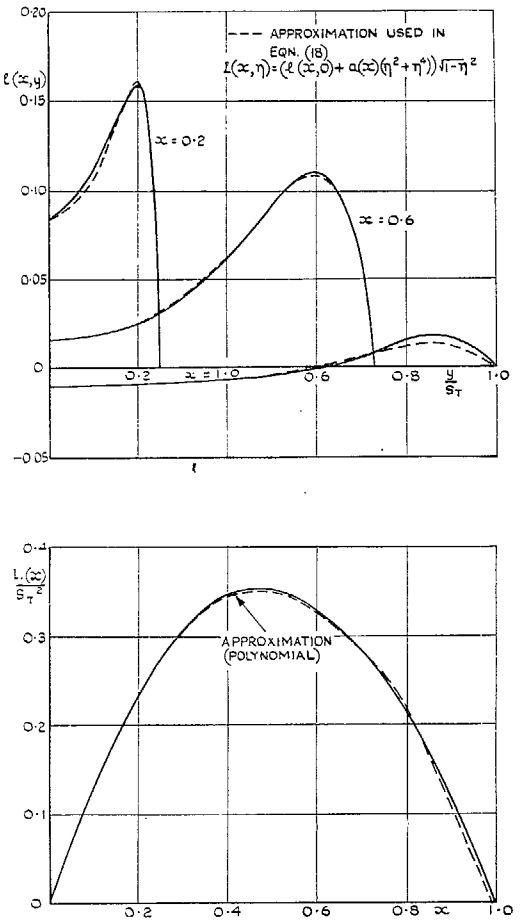

FIG. 17. Load distributions for example of Section 5.2.

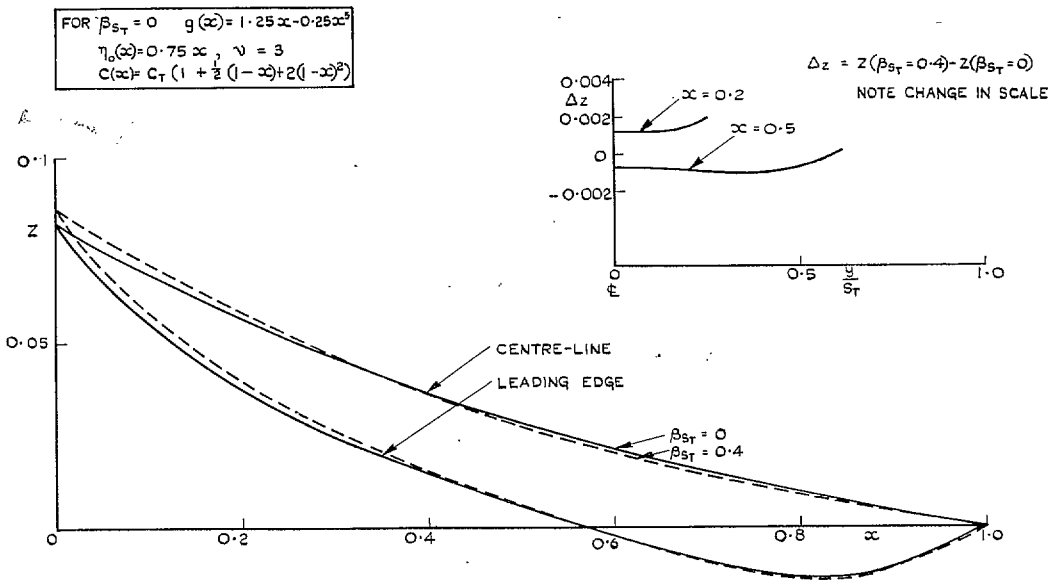

FIG. 18. Change in wing shape for same load distribution at $\beta s_T = 0$ and $0{\cdot}4$.

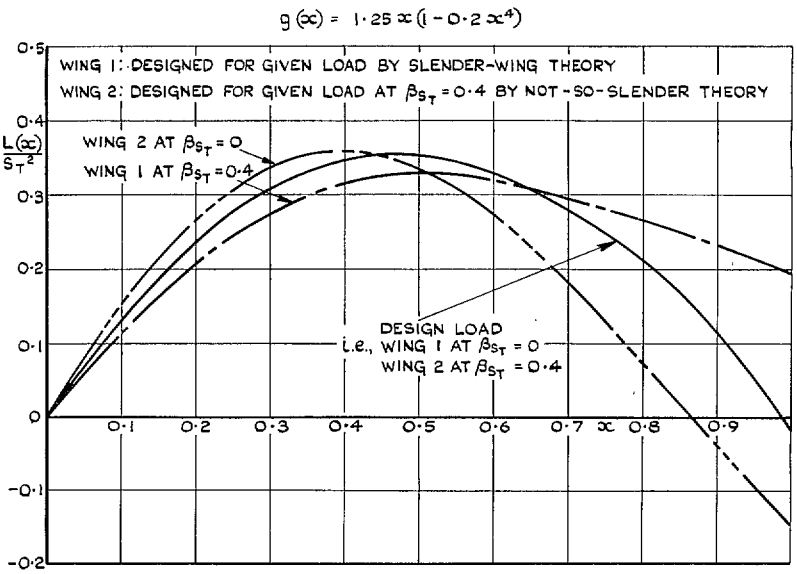

FIG. 19. Chordwise variation of spanwise load on cambered wings at different values of βs_T.

DETAILS OF TESTED WINGS:

$g(x) = 1{\cdot}25\ x\ (1 - 0{\cdot}2\,x^4)$: $S_T = 0{\cdot}25$.

BOTH WINGS HAVE DIAMOND CROSS-SECTION: 6·5 % THICK ON CENTRE-LINE.

WING 1 : SLENDER-WING DESIGN (FIG. 16)

WING 2 : NOT-SO-SLENDER WING DESIGN (FIG. 18)

THE EXPERIMENTAL RESULTS INCLUDE A CORRECTION FOR STING INTERFERENCE WHICH MAY BE IN ERROR BY 0·01 C_0.

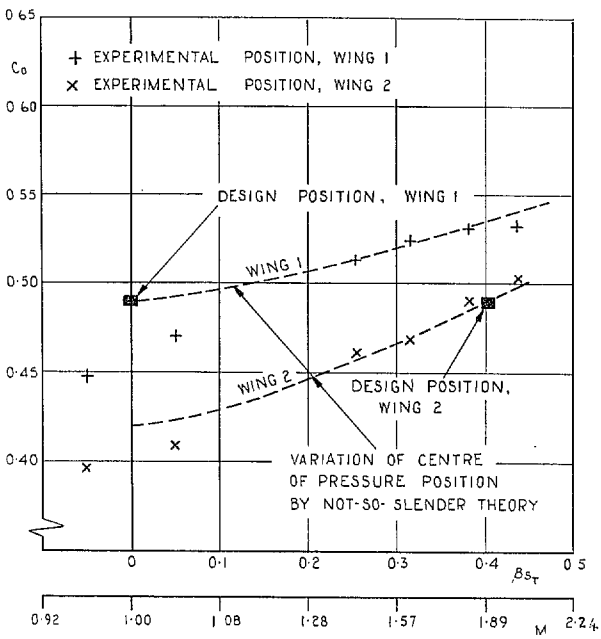

FIG. 20. Comparison of experimental and theoretical positions of centre of pressure at $C_L = 0{\cdot}05$.

(84810) Wt. 67/1876 K.5 6/62 Hw.

Publications of the Aeronautical Research Council

ANNUAL TECHNICAL REPORTS OF THE AERONAUTICAL RESEARCH COUNCIL (BOUND VOLUMES)

1942 Vol. I. Aero and Hydrodynamics, Aerofoils, Airscrews, Engines. 75*s.* (post 2*s.* 9*d.*)
Vol. II. Noise, Parachutes, Stability and Control, Structures, Vibration, Wind Tunnels. 47*s.* 6*d.* (post 2*s.* 3*d.*)

1943 Vol. I. Aerodynamics, Aerofoils, Airscrews. 80*s.* (post 2*s.* 6*d.*)
Vol. II. Engines, Flutter, Materials, Parachutes, Performance, Stability and Control, Structures. 90*s.* (post 2*s.* 9*d.*)

1944 Vol. I. Aero and Hydrodynamics, Aerofoils, Aircraft, Airscrews, Controls. 84*s.* (post 3*s.*)
Vol. II. Flutter and Vibration, Materials, Miscellaneous, Navigation, Parachutes, Performance, Plates and Panels, Stability, Structures, Test Equipment, Wind Tunnels. 84*s.* (post 3*s.*)

1945 Vol. I. Aero and Hydrodynamics, Aerofoils. 130*s.* (post 3*s.* 6*d.*)
Vol. II. Aircraft, Airscrews, Controls. 130*s.* (post 3*s.* 6*d.*)
Vol. III. Flutter and Vibration, Instruments, Miscellaneous, Parachutes, Plates and Panels, Propulsion. 130*s.* (post 3*s.* 3*d.*)
Vol. IV. Stability, Structures, Wind Tunnels, Wind Tunnel Technique. 130*s.* (post 3*s.* 3*d.*)

1946 Vol. I. Accidents, Aerodynamics, Aerofoils and Hydrofoils. 168*s.* (post 3*s.* 9*d.*)
Vol. II. Airscrews, Cabin Cooling, Chemical Hazards, Controls, Flames, Flutter, Helicopters, Instruments and Instrumentation, Interference, Jets, Miscellaneous, Parachutes. 168*s.* (post 3*s.* 3*d.*)
Vol. III. Performance, Propulsion, Seaplanes, Stability, Structures, Wind Tunnels. 168*s.* (post 3*s.* 6*d.*)

1947 Vol. I. Aerodynamics, Aerofoils, Aircraft. 168*s.* (post 3*s.* 9*d.*)
Vol. II. Airscrews and Rotors, Controls, Flutter, Materials, Miscellaneous, Parachutes, Propulsion, Seaplanes, Stability, Structures, Take-off and Landing. 168*s.* (post 3*s.* 9*d.*)

1948 Vol. I. Aerodynamics, Aerofoils, Aircraft, Airscrews, Controls, Flutter and Vibration, Helicopters, Instruments, Propulsion, Seaplane, Stability, Structures, Wind Tunnels. 130*s.* (post 3*s.* 3*d.*)
Vol. II. Aerodynamics, Aerofoils, Aircraft, Airscrews, Controls, Flutter and Vibration, Helicopters, Instruments, Propulsion, Seaplane, Stability, Structures, Wind Tunnels. 110*s.* (post 3*s.* 3*d.*)

Special Volumes

Vol. I. Aero and Hydrodynamics, Aerofoils, Controls, Flutter, Kites, Parachutes, Performance, Propulsion, Stability. 126*s.* (post 3*s.*)
Vol. II. Aero and Hydrodynamics, Aerofoils, Airscrews, Controls, Flutter, Materials, Miscellaneous, Parachutes, Propulsion, Stability, Structures. 147*s.* (post 3*s.*)
Vol. III. Aero and Hydrodynamics, Aerofoils, Airscrews, Controls, Flutter, Kites, Miscellaneous, Parachutes, Propulsion, Seaplanes, Stability, Structures, Test Equipment. 189*s.* (post 3*s.* 9*d.*)

Reviews of the Aeronautical Research Council

1939–48 3*s.* (post 6*d.*) 1949–54 5*s.* (post 5*d.*)

Index to all Reports and Memoranda published in the Annual Technical Reports

1909–1947 R. & M. 2600 (out of print)

Indexes to the Reports and Memoranda of the Aeronautical Research Council

Between Nos. 2351–2449	R. & M. No. 2450 2*s.* (post 3*d.*)
Between Nos. 2451–2549	R. & M. No. 2550 2*s.* 6*d.* (post 3*d.*)
Between Nos. 2551–2649	R. & M. No. 2650 2*s.* 6*d.* (post 3*d.*)
Between Nos. 2651–2749	R. & M. No. 2750 2*s.* 6*d.* (post 3*d.*)
Between Nos. 2751–2849	R. & M. No. 2850 2*s.* 6*d.* (post 3*d.*)
Between Nos. 2851–2949	R. & M. No. 2950 3*s.* (post 3*d.*)
Between Nos. 2951–3049	R. & M. No. 3050 3*s.* 6*d.* (post 3*d.*)
Between Nos. 3051–3149	R. & M. No. 3150 3*s.* 6*d.* (post 3*d.*)

HER MAJESTY'S STATIONERY OFFICE

from the addresses overleaf

Printed and published by
HER MAJESTY'S STATIONERY OFFICE

To be purchased from
York House, Kingsway, London W.C.2
423 Oxford Street, London W.1
13A Castle Street, Edinburgh 2
109 St. Mary Street, Cardiff
39 King Street, Manchester 2
50 Fairfax Street, Bristol 1
35 Smallbrook, Ringway, Birmingham 5
80 Chichester Street, Belfast 1
or through any bookseller

Printed in England

S.O. Code No. 23-3278